Published OnlineFirst April 15, 2019; DOI: 10.1158/2326-6066.CIR-18-0505

Research Article

Cancer Immunology Research

Siglec-9 Regulates an Effector Memory CD8$^+$ T-cell Subset That Congregates in the Melanoma Tumor Microenvironment

Quentin Haas[1], Kayluz Frias Boligan[1], Camilla Jandus[1,2], Christoph Schneider[1], Cedric Simillion[3], Michal A. Stanczak[4,5], Monika Haubitz[6], Seyed Morteza Seyed Jafari[7], Alfred Zippelius[4,5], Gabriela M. Baerlocher[6,8], Heinz Läubli[4,5], Robert E. Hunger[7], Pedro Romero[2], Hans-Uwe Simon[1], and Stephan von Gunten[1]

Abstract

Emerging evidence suggests an immunosuppressive role of altered tumor glycosylation due to downregulation of innate immune responses via immunoregulatory Siglecs. In contrast, human T cells, a major anticancer effector cell, only rarely express Siglecs. However, here, we report that the majority of intratumoral, but not peripheral blood, cytotoxic CD8$^+$ T cells expressed Siglec-9 in melanoma. We identified Siglec-9$^+$ CD8$^+$ T cells as a subset of effector memory cells with high functional capacity and signatures of clonal expansion. This cytotoxic T-cell subset was functionally inhibited in the presence of Siglec-9 ligands or by Siglec-9 engagement by specific antibodies. TCR signaling pathways and key effector functions (cytotoxicity, cytokine production) of CD8$^+$ T cells were suppressed by Siglec-9 engagement, which was associated with the phosphorylation of the inhibitory protein tyrosine phosphatase SHP-1, but not SHP-2. Expression of cognate Siglec-9 ligands was observed on the majority of tumor cells in primary and metastatic melanoma specimens. Targeting the tumor-restricted, glycosylation-dependent Siglec-9 axis may unleash this intratumoral T-cell subset, while confining T-cell activation to the tumor microenvironment.

Introduction

Breakthroughs in T-cell–based immunotherapeutic strategies have led to unprecedented and long-lasting clinical responses in a growing number of patients with advanced-stage melanoma and in an increasing number of other cancers (1, 2). Clinical responses have been achieved by immune-checkpoint therapies targeting inhibitory receptors on CD8$^+$ T cells in order to exploit their antitumor effector functions (1–4). These results also highlight the importance of cytotoxic CD8$^+$ T cells and the need to understand the mechanisms that restrain this population (5–8).

Altered tumor cell–surface glycosylation is common and has been extensively exploited for diagnostic purposes (9), such as the detection of cancer antigen (CA) 15-3, CA 19-9, and CA 125, yet evidence also suggests a role for glycosylation in cancer immunity (10, 11). A frequent feature in cancer is hypersialylation, the overexpression of sialic acids, which are considered markers of "self" and have been referred to as self-associated molecular patterns (SAMP; refs. 10, 12). By recognizing specific sialic acid–containing glycans (sialoglycans), inhibitory CD33-related Siglecs, which contain at least one classic immunoreceptor tyrosine-based inhibition motif (ITIM; refs. 13, 14), downregulate antitumor responses of innate immune cells, including NK cells, macrophages, or neutrophils (15–18). Siglecs specifically recognize certain sialoglycans based on their chemical structure, yet the identity and the tissue expression of Siglec ligands remain to be explored. However, evidence from lectin staining assays (16, 19) or from biosynthetic pathway expression analysis based on data from The Cancer Genome Atlas (TCGA; ref. 20) suggests overexpression of distinct Siglec ligands in different types of cancer. The tumor-associated antigen MUC1 has been identified as a ligand of Siglec-9 (18).

In contrast to other hominids, only a minority of circulating human T cells express Siglec-9 (21, 22), and structural differences of CD33-related Siglecs, involving gene deletion, gene conversion, or changes in binding specificity, have been linked to evolutionary changes in the sialome (23). Here, we demonstrated that the majority of tumor-infiltrating CD8$^+$ T cells in melanoma specimens expressed Siglec-9. These Siglec-9–expressing tumor-infiltrating lymphocytes (TIL), as well as circulating Siglec-9$^+$ CD8$^+$ T cells from melanoma patients and healthy donors, exhibited an effector memory phenotype. Despite the

[1]Institute of Pharmacology, University of Bern, Bern, Switzerland. [2]Department of Oncology UNIL CHUV, University of Lausanne, Lausanne, Switzerland. [3]Department for BioMedical Research (DBMR), University of Bern, Bern, Switzerland. [4]Cancer Immunology Laboratory, Department of Biomedicine, University Hospital Basel, Basel, Switzerland. [5]Division of Oncology, Department of Internal Medicine, University Hospital Basel, Basel, Switzerland. [6]Experimental Hematology, Department of BioMedical Research, University of Bern, Bern, Switzerland. [7]Department of Dermatology, Inselspital, Bern University Hospital, Bern, University of Bern, Bern, Switzerland. [8]Department of Hematology, University Hospital of Bern, Bern, Switzerland.

Note: Supplementary data for this article are available at Cancer Immunology Research Online (http://cancerimmunolres.aacrjournals.org/).

Corresponding Author: Stephan von Gunten, University of Bern, 3012 Bern, Switzerland. Phone: 41-31-632-32-98; Fax: 41-31-632-49-94. E-mail: stephan.vongunten@pki.unibe.ch

doi: 10.1158/2326-6066.CIR-18-0505

Published OnlineFirst April 15, 2019; DOI: 10.1158/2326-6066.CIR-18-0505

coexpression of inhibitory receptors, including PD-1, Siglec-9$^+$ CD8$^+$ T cells exhibited high proliferative and functional capabilities upon polyclonal activation *in vitro*. However, engagement by Siglec-9–specific antibodies or Siglec-9 ligands on target cells resulted in suppressed TCR signaling and effector functions, indicating the regulatory capacity of Siglec-9. Agonistic stimulation of Siglec-9 was associated with phosphorylation of the inhibitory phosphatase SHP-1, but not SHP-2, in human primary CD8$^+$ T cells. We observed that the majority of melanoma cells in both primary and metastatic lesions expressed cognate sialoglycan ligands of Siglec-9. Thus, Siglec-9 receptor–ligand interactions may result in a tumor glycosylation-dependent inhibitory circuit that functions to suppress T-cell effector responses in the tumor microenvironment.

Materials and Methods

Cells and tissues

Blood from healthy donors ($n = 60$) and melanoma patients ($n = 8$) was collected upon written informed consent or buffy coats were purchased from the Blood Transfusion Center of Bern, Switzerland. All donors were older than 18 years. Donors with a history of blood or immunologic disorder, or donors receiving immunomodulatory drugs or chemotherapeutic interventions within 6 months before blood withdrawal, were excluded. Only patients with histologically confirmed metastatic malignant melanoma were included. Peripheral blood mononuclear cells (PBMC) were obtained by density centrifugation using Pancoll solution (PAN-Biotech). For functional experiments, CD8$^+$ T cells were isolated using the EasySep Human CD8$^+$ T-Cell Isolation Kit (STEMCELL Technologies), according to the manufacturer's instructions. Purity of isolated cells was always >95%. For experiments with Siglec-9$^+$ and Siglec-9$^-$ CD8$^+$ T-cell subsets, cells were isolated using fluorescence-activated cell sorting (FACSAria, BD Biosciences) using antibody against siglec-9 (FAB1139A, R&D Systems). The purity of each sorted subset was >99%.

Written informed consent was obtained from all patients prior to tissue sample collection. Surgical specimens were mechanically dissociated and digested in RPMI (Sigma-Aldrich) supplemented with accutase at 1:1 dilution in medium (L11-007; PAA Laboratories), collagenase IV (1 mg/mL), hyaluronidase (1 mg/mL; Millipore Sigma), and DNAse type I (10 U/mL; Millipore Sigma), filtered (Corning cell strainer, 40 µm; Sigma-Aldrich), washed in RPMI medium containing 10% fetal calf serum (FCS; Life Technologies) and 1% penicillin/streptomycin (Life Technologies). Cells were frozen for future analysis in FCS containing 10% dimethyl sulfoxide (Sigma-Aldrich).

Melanoma tissue microarrays were purchased from US Biomax and contained primary melanoma, metastatic melanoma, and control tissues (intradermal nevus). All studies using human material were in accordance with the guidelines of, and approved by the cantonal ethical committees of, Bern and Basel, Switzerland. Written informed consent was received from participants prior to inclusion in the study.

Cell lines

The human melanoma cell line Me275 (established at the Ludwig Cancer Institute in Lausanne Switzerland, provided by Pedro Romero) and the human acute monocytic leukemia cell line THP1 (ATCC) were cultured in RPMI medium (Sigma-Aldrich) containing 10% FCS (Life Technologies) and 1% penicillin/streptomycin (Life Technologies). Both human cell lines were used exclusively between passages 3 and 6. THP1 cell line authentication was performed by Microsynth by the short-tandem repeat method (PowerPlex16, Promega). For the redirected cytotoxic assay, the mouse mastocytoma cell line P815 (from ATCC) was used exclusively between passage 5 and 8. This cell line was authenticated by the short-tandem repeat method but not further authenticated in the past years. The cell line was cultured in DMEM (Sigma-Aldrich) containing 10% FCS; Life Technologies) and 1% penicillin/streptomycin (Life Technologies), supplemented or not with murine IFNγ (1,000 U/mL; PeproTech). No *Mycoplasma* testing was performed for the cell lines.

Cell culture

Isolated CD8$^+$ T cells were cultured in RPMI medium (Sigma-Aldrich) containing 10% FCS (Life Technologies) and 1% penicillin/streptomycin (Life Technologies) supplemented with rhIL2 (100 U/mL; PeproTech). When required, cells were activated with plate-bound anti-CD3 (1 µg/mL; OKT-3, Bio X Cell) and soluble anti-CD28 (1 µg/mL, BioLegend) for 1 hour at 37°C in supplemented medium and cultured in the presence or absence of IL12 (50 ng/mL), IL21 (20 ng/mL), IL5 (20 ng/mL), IL10 (40 ng/mL), IL15 (100 ng/mL), IL18 (100 ng/mL), or LPS (100 ng/mL; all from PeproTech).

Flow cytometry

PBMCs, lymphocytes isolated from melanoma tissues, or purified CD8$^+$ T cells were labeled using fluorescent mAbs directed against surface molecules (20 minutes at 4°C), washed in PBS with 0.2% BSA (Sigma-Aldrich), and acquired using a FACSVerse (BD Biosciences). A minimum of 100,000 cells were used for each staining. When required, cells were blocked using FC-block (human Trustain FcX, BioLegend), and viability was analyzed using the Zombie NIR viability kit (BioLegend). Cells were labeled either directly *ex vivo* or, where indicated, after 30 minutes of treatment with neuraminidase (25 mU; Roche Diagnostics) at 37°C. Intracellular cytokine staining was done at 4°C for 30 minutes.

Isolated CD8$^+$ T cells were stimulated for 1 hour at 37°C in 5% CO_2 with anti-CD3 (1 µg/mL, plate bound) and anti-CD28 (1 µg/mL, soluble) or with anti-CD3 mAb-coated P815 cells. Thereafter, GolgiPlug and GolgiStop (BD Biosciences) were added to the cultures followed by incubation for 5 hours. Cells were spun down and incubated with fluorochrome-conjugated mAbs against surface markers. Cells were then washed, fixed with 2% paraformaldehyde in PBS, permeabilized in PBS supplemented with 2% heat-inactivated FCS, 2 mmol/L EDTA, and 0.5% saponin (all from Sigma-Aldrich), and stained intracellularly with fluorochrome-conjugated mAbs against cytokines TNFα (MAB11, eBioscience) and IFNγ (4S.B3, BioLegend) or ZAP-70 (PY292, J34-602, BD Biosciences) and SLP-76 (PY128, J141-668.36.58, BD Biosciences). Finally, cells were washed in PBS and analyzed on a BD FACSVerse (BD Biosciences). Data were analyzed with FlowJo 10.0.6 software (Tree Star Inc.).

For surface staining, fluorochrome-conjugated antibodies against CCR3 (5.E.8), CCR5 (HEK/1/85a), CXCR6 (TG3/CXCR6), CCR9 (L053E8), Integrin $\alpha_4\beta_7$ (FIB27), BTLA (MIH26), PD-1 (EH12.1), CTLA-4 (BNI3), Tim-3 (7D3), mouse PD-L1 (MIH5), and mouse PD-L2 (TY25) were purchased from BioLegend. The fluorochrome-conjugated antibodies against CD3

Published OnlineFirst April 15, 2019; DOI: 10.1158/2326-6066.CIR-18-0505

(SK7), CD8 (RPA-T8), CLA (HECA-452), TCRαβ (IP26), CD45RA (HI100), LAG3 (T47-530), CXCR3 (1C6/CXCR3), CCR4 (1G1), CD107a (H4A3), ZAP-70 (PY292, J34-602), SLP-76 (PY128, J141-668.36.58), and CCR7 (G043H7) were purchased from BD Biosciences, whereas Siglec-9 (191240), CCR1 (53504), and CCR7 (150503) were from R&D Systems. Each mAb was titrated on PBMCs before use. Data analysis was performed using FlowJo (V10.4.2, Tree Star Inc.).

Immunostaining of tissue sections

Detection of Siglec-9 ligands by immunofluorescence was performed as previously described (16). Paraffin-embedded tissue sections from melanoma or tissue microarrays (TMA) were deparaffinized with NeoClear (Millipore Sigma) and graded ethanol (ranging from 100% to 40%). Antigen retrieval was performed by heating the sections in 0.1 mol/L citrate buffer (Dako) pH 6.0 three times for 3 minutes in a microwave, with intermediate cooling 8 incubations of 20 minutes. For the Siglec-9 ligands staining, recombinant human Siglec-9 hFc (10 μg/mL; R&D Systems) was preincubated with PE-conjugated goat anti-human Ig (polyclonal, Jackson ImmunoResearch Laboratories) diluted 1/100 in PBS containing 10% FCS (Life Technologies) and 1% penicillin/streptomycin (Life Technologies) for 1 hour at 4°C and then applied to the tissue samples for 1 hour at room temperature. For the selection of specific tumor areas, the tissue samples were costained with the melanoma marker 13 melan-A (Dako). Sections were incubated with 4′,6-Diamidin-2-phenylindol (DAPI, Thermo Fisher Scientific) for nuclei detection and mounted in ProLongTM Gold Antifade Reagent (Invitrogen). Stained samples were scanned using a Pannoramic MIDI slide scanner (3DHISTECH) or by confocal microscopy (LSM 700; Carl Zeiss). Acquired images were analyzed using 17 the ImageJ software version 1.51 (NIH) or QuPath (24).

Telomere length measurement by automated multicolor flow-FISH 20

For telomere length analysis, human CD8$^+$ T-cell Siglec-9$^+$ and Siglec-9$^-$ subsets were isolated from the peripheral blood of 3 healthy donors by fluorescence-activated cell sorting as described above. Telomere length measurement by *in situ* hybridization and flow cytometry (automated multicolor flow-FISH) was then performed as previously described (16). A total of 2.5×10^3 to 2×10^6 cells were used for *in situ* hybridization. Cells were incubated with 170 μL hybridization mixture containing 75% deionized formamide (Sigma-Aldrich), 20 mmol/L Tris (pH 7.1; Sigma-Aldrich), and 1% BSA (Sigma-Aldrich) with no probe (unstained) or with telomere-specific FITC-conjugated $(C_3TA_2)_3$ peptide nucleic acid (PNA; 0.3 μg/mL; Applied Biosystems). Denaturation was done at 87°C for 15 minutes, and hybridization was performed in the dark and at room temperature for 90 minutes. Excess and nonspecifically bound telomere PNA probe was removed by 4 washing steps at room temperature using 1 mL washing solution containing 75% formamide, 10 mmol/L Tris, 0.1% BSA, and 0.1% Tween 20 (Sigma-Aldrich), followed by washing with 1 mL solution containing PBS, 0.1% BSA, and 0.1% Tween 20 at room temperature. DNA counterstaining was performed using a solution containing Sheath Fluid (BD Biosciences), 0.1% BSA, and a subsaturating amount of LDS 751 (0.01 36 μg/mL; Invitrogen) overnight. Acquisition of telomere fluorescence was performed using FACSCalibur (BD Biosciences). For each sample, unstained and telomere stained samples were tested. FlowJo version 10 (Tree Star Inc.) was used for analysis of telomere length in the specific cell subsets. Specific telomere fluorescence was determined as the difference between the fluorescence of the stained samples minus the (auto-) fluorescence of the corresponding unstained sample. Using calibration beads and an internal standard of cow thymocytes, the telomere fluorescence was calculated into kilobases of telomere length.

Immunoblotting

For immunoblotting analysis antibodies against phosphorylated SHP-1 (polyclonal) and total SHP-1 (clone Y476) were both purchased from Abcam and diluted 1/1000 in PBS supplemented with 0.05% Tween (Sigma-Aldrich) and 5% BSA. Antibodies against phosphorylated SHP-2 (polyclonal) and total SHP-2 (clone D50F2) were purchased from Cell Signaling Technologies and diluted 1/1000 in PBS supplemented with 0.05% Tween (Sigma-Aldrich) and 5% BSA. Siglec-9 agonistic antibody (E10-286) was provided by BD Pharmingen and used at an optimized concentration of 3 μg/mL. Capturing Siglec-9 antibodies were provided by R&D Systems. For the detection of SHP-1 and SHP-2 phosphorylation, CD8$^+$ T cells were stimulated with agonistic anti–siglec-9 (E10-286) or isotype control (3 μg/mL, mouse IgG1, clone MG1-45, BD Biosciences) for different time points. Thereafter, the cells were harvested, washed, and lysed on ice for 30 minutes in RIPA buffer with protease inhibitor (P8340) and phosphatase inhibitor (P5726) cocktails (all from Sigma-Aldrich) diluted 1/100. The cell lysates were cleared by centrifugation at 14,000 rpm for 15 minutes. Protein content of samples was assessed by the Pierce BCA protein assay kit (Thermo Fisher Scientific), and 20 μg of total proteins per well was used for the assay. Lysates were boiled for 5 minutes, proteins were separated by SDS-PAGE, and transferred to PVDF membranes. Membranes were blocked with 5% BSA (Sigma-Aldrich) and probed overnight with antibodies against total or phosphorylated SHP-1 or pSHP-2. In all cases, the signal was detected using an anti-rabbit-HRP secondary antibody (GE Healthcare) diluted 1/10,000 in PBS supplemented with 0.05% Tween (Sigma-Aldrich) and 5% BSA and revealed by the addition of Luminata Forte (Millipore) according to the manufacturer's protocol. Exposure was done using an Odyssey Infrared Imaging System (LI-COR Biosciences).

RNA analysis on TCGA database

Data were obtained from TCGA-SKCM project (Project ID; dbGaP Study Accession: phs000178). There was no inclusion or exclusion criteria applied. The study represents 469 patients. The results shown here are based upon data generated by the TCGA Research Network: http://cancergenome.nih.gov/. The publicly available TCGA data sets were downloaded from the TCGA Data Portal at https://tcga-data.nci.nih.gov/tcga/. The detailed information of the TCGA data structures can be reviewed at https://tcga-data.nci.nih.gov/tcga/tcgaDataType.jsp. The detailed information of the RNA-seq experiments, protocols, and software used can be found at the TCGA Data Portal at https://tcga-data.nci.nih.gov/tcga/. Data were retrieved on August 21, 2017. Values represent normalized and log-transformed read counts (log-transformed RPKM values). Figures were created in R version 3.4.2 (Bell Laboratories, formerly AT&T, now Lucent Technologies) using the heatmap2 and the ggplot2 library. Dendrogram clustering algorithm was used for Fig. 2. The ranking of cliques as high, moderate, and low expression in Fig. 2 is an arbitrary denomination to distinguish the cliques; no preliminary cutoff was determined.

Published OnlineFirst April 15, 2019; DOI: 10.1158/2326-6066.CIR-18-0505

Proliferation assay

Purified human CD8$^+$ T cells were labeled with a final concentration of 5 μmol/L CFSE (Molecular Probes, Thermo Fisher Scientific) according to the manufacturer's instructions. Cells were activated using anti-CD3 and anti-CD28 as described above and cultured in complete RPMI medium supplemented with rhIL2 (100U/mL, PeproTech). CFSE fluorescence was evaluated at day 4 by flow cytometry.

CD107a mobilization assay

Purified human CD8$^+$ T cells were incubated at a 3:1 ratio with P815 target cells for 4 hours, in the presence of FITC-conjugated anti-CD107a (BioLegend) in a dilution of 2/100. After incubation, cells were washed with PBS plus 0.2% BSA (Sigma-Aldrich) and analyzed on a FACSVerse (BD Biosciences). Where indicated, target cells were pretreated with neuraminidase (25 mU; Roche Diagnostics) for 30 minutes at 37°C and washed extensively before coculture with CD8$^+$ T cells.

Redirected cytotoxicity assay

Cytolytic CD8$^+$ T-cell activity was evaluated in a redirected cytotoxicity assay against P815 cells. To this end, the P815 cells were incubated with anti-CD3 (20 μg/mL; OKT-3) for 1 hour. When indicated, P815 cells were treated with neuraminidase (25 mU, Roche Diagnostics). CD3-coated P815 cells were cocultured (3:1 E/T ratio) with CD8$^+$ T cells pretreated or not with monoclonal anti–PD-1 (10 μg/mL, pembrozilumab, Merck and Co) for 30 minutes at 37°C. After 4 hours of incubation, the specific lysis of P815 cells was assessed by measuring the LDH activity in the supernatant, with the Cytotoxicity Detection Kit^{PLUS} LDH (Roche Diagnostics), according to the manufacturer's instructions. Specific lysis was calculated as (experimental – spontaneous release)/(total – spontaneous release)*100 and expressed as a fold change between treated and untreated groups (specific lysis fold change).

Enzyme-linked immunosorbent assay (ELISA)

High-binding polystyrene microtiter plates (Thermo Fisher Scientific) were coated with anti–siglec-9 (100 μL at 10 μg/mL; R&D Systems) in coating buffer (buffer composed of 0.795 g/mL Na_2CO_3 diluted in water, where a solution of 146.5 g/mL $NaHCO_3$ in water was added until pH reached 9.6) at 4°C overnight. Plates were washed 3 times with PBS, 5% Tween-20, and then blocked with 100 μL PBS-5% BSA for 1 hour at 37°C and washed an additional 3 times. Cell samples were lysed for 30 minutes at 4°C in NP40 Cell Lysis Buffer (Thermo Fisher Scientific) supplemented with protease inhibitor and phosphatase inhibitor cocktails (all from Sigma-Aldrich). Protein concentration of samples was determined using Pierce BCA protein assay kit (Thermo Fisher Scientific) according to the manufacturer's instructions. Sample lysates (100 μL) diluted in blocking solution to randomize concentrations were added to the wells for 2 hours at room temperature. After washing 3 times, 100 μL of anti–phospho-tyrosine-HRP (R&D Systems) diluted 5,000 times in blocking buffer was added for 2 hours at room temperature. After washing 3 times, 100 μL of 3,3′,5,5′-tetramethylbenzidine (TMB; Sigma-Aldrich) was added for 10 minutes. Fifty microliters of 1 mol/L HCl stop solution was added before reading on Odyssey Infrared Imaging System (LI-COR Biosciences).

TCRVβ sequencing

CD8$^+$ T cells were isolated from peripheral blood of healthy donors and TILs and separated by fluorescence-activated cell sorting into Siglec-9$^+$ and Siglec-9$^-$ populations as already described. Genomic DNA from Siglec-9$^+$ and Siglec-9$^-$ subsets was extracted using the NucleoSpin Tissue kit from Macherey-Nagel according to the manufacturer's instructions. Genomic DNA quantity and purity were assessed through spectrometric analysis. A total of 1.47 to 29.1 ng/μL of genomic DNA was analyzed by high-throughput sequencing of the TCRVβ using the ImmunoSEQ immune profiling platform at the survey level (Adaptive Biotechnologies), which represents a detection capacity of 1 cell in 40,000. Raw sequence reads were demultiplexed according to Adaptive's proprietary barcode sequences. Demultiplexed reads were then further processed to remove adapter and primer sequences, identify and correct for technical errors introduced through PCR and sequencing, and remove primer dimer, germline, and other contaminant sequences. The data are filtered and clustered using both the relative frequency ratio between similar clones and a modified nearest-neighbor algorithm, to merge closely-related sequences. The resulting sequences were sufficient to allow annotation of the V(*N*)D(N)J genes constituting each unique CDR3 and the translation of the encoded CDR3 amino acid sequence. V, D, and J gene definitions were based on annotation in accordance with the IMGT database (www.imgt.org). Data were analyzed using the immunoSEQ Analyzer toolset. Data are available on the following link: https://clients.adaptivebiotech.com/pub/haas-2019-cir.

Statistical analysis

Unless otherwise indicated, data represent mean ± standard deviation (SD). For quantitative comparisons, Student *t* test (2-sample 2-tailed comparison) or one-way ANOVA with Holm–Sidak or Bonferroni posttest (multiple-sample comparison) was performed using Prism 5.0. $P < 0.05$ was considered significant.

Data sharing statement

For original data, please contact stephan.vongunten@pki.unibe.ch.

Results

Tumor-infiltrating effector memory CD8$^+$ T cells express Siglec-9

CD8$^+$ T cells are considered as major anticancer effector cells (25, 26). We observed that the percentage of peripheral blood siglec-9$^+$ CD8$^+$ T cells was low in melanoma patients ($n = 8$) and healthy individuals ($n = 23$; Fig. 1A and B), which is in line with previous reports of low expression of Siglecs on circulating T cells (21, 22). In contrast, the majority of tumor-infiltrating CD8$^+$ T cells from melanoma patients ($n = 6$) expressed Siglec-9, and neuraminidase treatment, which has been shown by us to unmask Siglecs on NK cells bound by sialic acid ligands *in cis* (16), had no effect on the Siglec-9 staining of healthy individual CD8$^+$ T cells (Supplementary Fig. S1). An analysis of tumors from the TCGA melanoma data set revealed that CD8α and CD8β (Fig. 1C), but not NKp46 expression (Supplementary Fig. S2) correlated significantly with *SIGLEC9* gene expression.

We went on to investigate phenotypic and functional characteristics of Siglec-9$^+$ CD8$^+$ T cells. Flow-cytometric analysis based on CCR7 and CD45RA cell-surface expression (27) revealed that

Published OnlineFirst April 15, 2019; DOI: 10.1158/2326-6066.CIR-18-0505

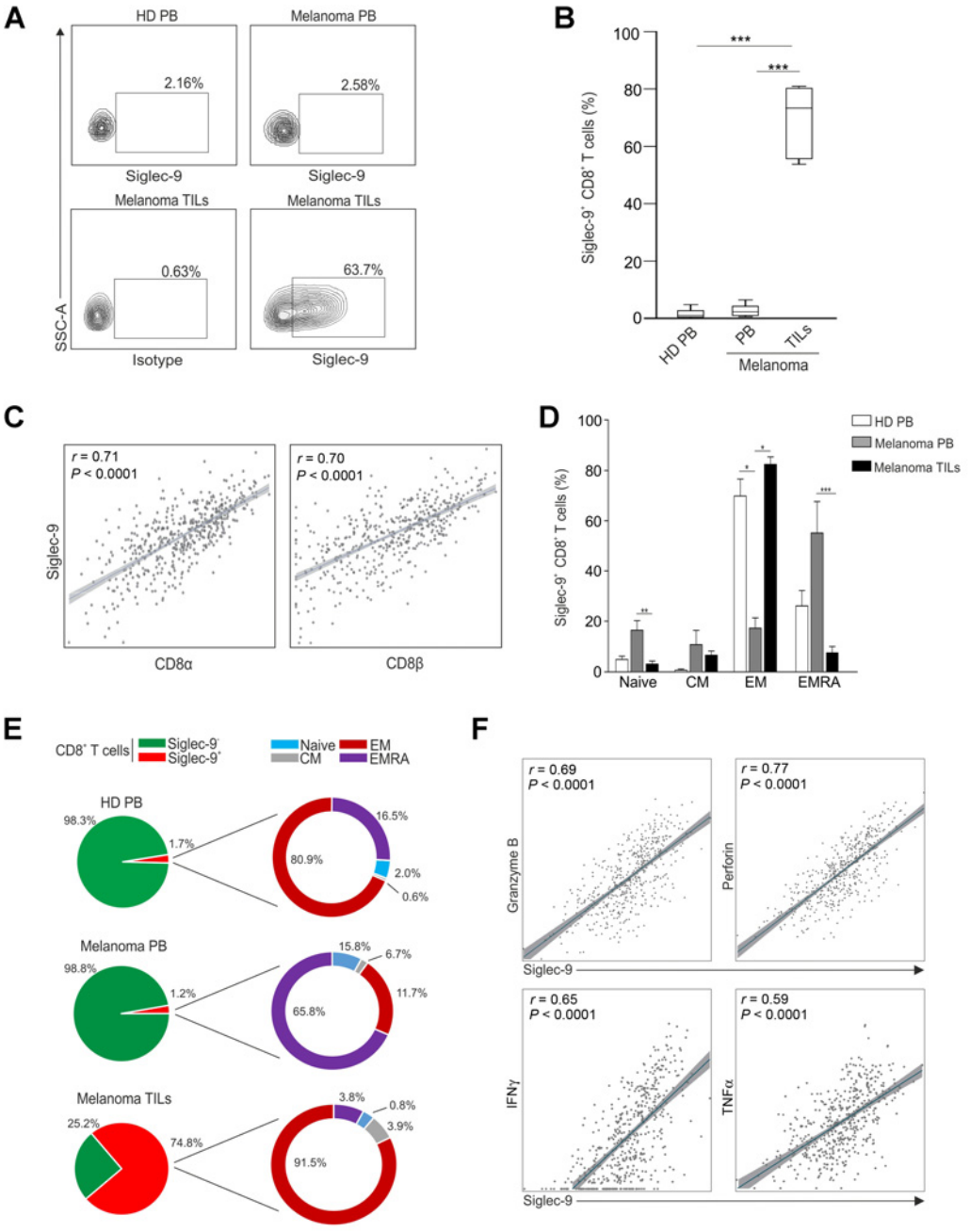

Figure 1.

Siglec-9 defines a subset of EM CD8$^+$ T cells that prevails in the melanoma tumor microenvironment. **A,** Representative flow cytometry plots of Siglec-9 on CD8$^+$ T cells from the peripheral blood (PB) of HD or melanoma patients, and melanoma TILs and (**B**) quantitative analysis of Siglec-9 on CD8$^+$ T cells from the PB of healthy donors ($n = 23$) or melanoma patients ($n = 8$), and melanoma TILs ($n = 6$). **C,** Pairwise scatter plot representation of RNA expression (log2) of Siglec-9 compared with CD8α and CD8β in melanoma specimens ($n = 469$), according to TCGA Network data. **D** and **E**, Flow-cytometric, multiparametric assessment of Siglec-9 surface expression on naïve, central memory (CM), effector memory (EM), and CD45RA$^+$ effector memory (EMRA) CD8$^+$ T-cell subsets in the PB of healthy donors ($n = 8$) or melanoma patients ($n = 6$), and melanoma TILs ($n = 5$); **D,** quantitative analysis and (**E**) illustration. **F,** Pairwise scatter plot representation of RNA expression of Siglec-9 compared with granzyme B, perforin, IFNγ, and TNFα in melanoma specimens ($n = 469$), according to TCGA Network data. Statistical analysis was performed by one-way ANOVA followed by followed by (**B**) Holm–Sidak or (**D**) Bonferroni posttest. Error bars, SD. *, $P < 0.05$; **, $P < 0.01$; ***, $P < 0.001$.

the subsets of Siglec-9$^+$ CD8$^+$ T cells in the peripheral blood of healthy donors and melanoma patients, as well as most Siglec-9$^+$ CD8$^+$ melanoma TILs, primarily exhibited an effector memory phenotype (Fig. 1D and E). Among these, the majority of Siglec-9$^+$ CD8$^+$ T cells in HD peripheral blood and patient TILs represented CCR7$^-$CD45RA$^-$ effector memory (EM) T cells, whereas

Published OnlineFirst April 15, 2019; DOI: 10.1158/2326-6066.CIR-18-0505

the majority of the circulating Siglec-9$^+$ CD8$^+$ T cells consisted of CCR7$^-$CD45RA$^+$ effector memory (EMRA) T cells in melanoma patients. In tumors of the TCGA melanoma data set, Siglec-9 mRNA expression correlated with enhanced transcription of the T-cell effector molecules granzyme B, perforin, IFNγ, and TNFα (Fig. 1F), resembling an activation-dependent inhibitory receptor expression program as previously reported (28–30).

Inhibition of Siglec-9$^+$ CD8$^+$ T-cell responses by tumor cell sialoglycan ligands

In a previous work, we found expression of Siglec-9 ligands on various human melanoma cell lines and in primary tissue specimens from five melanoma patients (16). Here, we expanded this analysis to include a tissue microarray (TMA) combined with lectin IHC using a recombinant Siglec-9–human IgG1 Fc chimera (16). We investigated Siglec-9 ligand expression in surgical resections from different patients, including primary ($n = 62$) and metastatic melanoma ($n = 20$) samples, as well as nonmalignant intradermal nevi (IDN; $n = 7$) specimens. In both primary and metastatic lesions, but not IDN, Siglec-9 ligands were found to be expressed, with a diffuse immunofluorescence staining pattern, on primary melanoma (mean 75.9%; range, 25.0%–97.8%) or metastatic (mean 63.4%; range, 25.3%–97.7%) melan-A$^+$ cells (Fig. 2A–C). In accordance with our previous report (16), Siglec-9 ligands were absent in normal tissue on the TMA (Fig. 2A).

The biosynthesis of specific Siglec ligands involves specific sialyltransferases (ST) that transfer sialic acids to acceptor carbohydrate residues in a linkage-dependent manner. Analysis of RNA-seq data from the TCGA database for the 20-known human STs in melanoma tumors ($n = 469$) revealed differential expression of the ST enzymes (Fig. 2D; Supplementary Fig. S3). Among the most expressed STs were ST3GAL5, ST6GALNAC2, and ST3GAL6, which are predicted to be key enzymes involved in the biosynthesis of Siglec-9 ligands as determined by glycan array technology at the Consortium for Functional Glycomics (http://www.functionalglycomics.org), and other techniques (31). Analysis of RNA-seq data from the TCGA database of melanoma tumors using a dendrogram clustering algorithm revealed a subgroup of seven STs, including ST3GAL5, ST6GALNAC2, and ST3GAL6, with consistently high expression in most melanoma specimens (clique 4), a subgroup of six STs with moderate expression (clique 3), and seven STs with low expression (cliques 1 and 2; Fig. 2D).

Next, we sought to examine the functional consequences of Siglec-9 engagement by its cognate ligands on T cells. P815 target cells used here express Siglec-9 ligands on their cell surface, as assessed by confocal microscopy (Fig. 2E). Enzymatic digestion using neuraminidase (sialidase) treatment was used to remove Siglec-9 sialoglycan ligands, as previously done (16). The redirected cytotoxic activity of Siglec-9$^+$ CD8$^+$ T cells from healthy donors was comparable with that of Siglec-9$^-$ cytotoxic T lymphocytes when cultured with anti-CD3–loaded P815 cancer cells (Fig. 2F). Enzymatic digestion of Siglec-9 surface ligands on the target cells by neuraminidase pretreatment only enhanced the cytotoxicity of the Siglec-9$^+$ cells. Following enzymatic digestion of Siglec-9 ligands on the target cells, Siglec-9$^+$ CD8$^+$ T cells from healthy donors constitutively responded to polyclonal activation with higher degranulation (CD107a mobilization; Fig. 2G) and intracellular cytokine production, including IFNγ and TNFα (Fig. 2H and I). Expression of Siglec-9 in Jurkat cells was previously reported to result in reduced phosphorylation of ZAP-70 following TCR engagement (21). Neuraminidase treatment of target cells resulted in enhanced TCR signaling exclusively within the healthy donor Siglec-9$^+$ CD8$^+$ T-cell subset, as evidenced by ZAP-70 (Fig. 2J) and SLP-76 (Fig. 2K) phosphorylation measurement.

Siglec-9 triggers SHP-1–associated inhibitory pathways in CD8$^+$ T cells

Engagement of Siglec-9 using the anti–Siglec-9 clone E10-286 has been previously shown to result in Siglec-9 phosphorylation (32) and agonistic effects on receptor functions (16, 32). In a redirected cytotoxicity assay, treatment with anti–Siglec-9 significantly reduced the killing activities of healthy donor-sorted Siglec-9$^+$, but not Siglec-9$^-$, CD8$^+$ T cells directed against anti-CD3–loaded P815 cells (Fig. 3A). Intracellular flow-cytometric analysis revealed that treatment with E10-286 also inhibited cytokine production, including IFNγ (Fig. 3B) and TNFα (Fig. 3C), exclusively in Siglec-9$^+$ CD8$^+$ T cells following costimulation by anti-CD3 and anti-CD28. Under these conditions, E10-286 stimulation also led to reduced phosphorylation of ZAP-70 (Fig. 3D) and SLP-76 (Fig. 3E) following TCR engagement. Given that Siglec-9 contains an ITIM known to recruit tyrosine phosphatases (21, 31, 33), the phosphorylation of Siglec-9, as well as the activation of the SH2 domain-containing protein tyrosine phosphatases SHP1 and SHP2, in CD8$^+$ T cells was investigated. Following Siglec-9 engagement by E10-286, rapid phosphorylation of Siglec-9 (Fig. 3F) and of SHP-1 (Fig. 3G; Supplementary Fig. S4) was observed with a peak after 5 minutes. In contrast, no significant phosphorylation of SHP-2 was observed (Fig. 3G; Supplementary Fig. S4). In line with this observation, in Jurkat cells, Siglec-9 has been shown to associate preferentially with SHP-1 and not SHP-2 (21). Phosphorylation of Siglec-9 appeared to occur in CD8$^+$ T cells isolated from patients TILs in comparison with unstimulated PBMCs from healthy donors (Supplementary Fig. S5). Melanoma tissue data from TCGA revealed a correlation between Siglec-9 and SHP-1, but not SHP-2 (Fig. 3H). These findings suggest a role of SHP-1–associated inhibitory pathways upon Siglec-9 engagement in CD8$^+$ T cells.

Functional Siglec-9$^+$ CD8$^+$ T cells derive from previous clonal expansion

We went on to assess the functional and phenotypic characteristics of the human Siglec-9$^+$ CD8$^+$ T-cell subset. Costimulation with anti-CD3 and anti-CD28 resulted in increased IFNγ and TNFα production by Siglec-9$^+$ CD8$^+$ T cells isolated from healthy donors, which was more prominent compared with their Siglec-9$^-$ counterparts (Fig. 4A and B). Flow-cytometric analysis of CD8$^+$ T-cell proliferation after anti-CD3 and anti-CD28 costimulation revealed a high proliferative capacity of the Siglec-9$^+$ CD8$^+$ T-cell subset (Fig. 4C). Together with the enhanced cytotoxicity and cytokine production observed in redirected assays (Fig. 2F–I), these data indicate that Siglec-9$^+$ CD8$^+$ T cells are functionally competent upon anti-CD3 and anti-CD28 stimulation *in vitro*.

Telomere length analysis was performed using automated multicolor flow-FISH, as previously done (16, 34). The results revealed evidence for multiple rounds of prior cell division within the Siglec-9$^+$ CD8$^+$ T cells of healthy individuals, indicating past proliferative responses of these cells (Fig. 4D). This subset demonstrated a higher cell-surface expression of chemokine receptors,

Published OnlineFirst April 15, 2019; DOI: 10.1158/2326-6066.CIR-18-0505

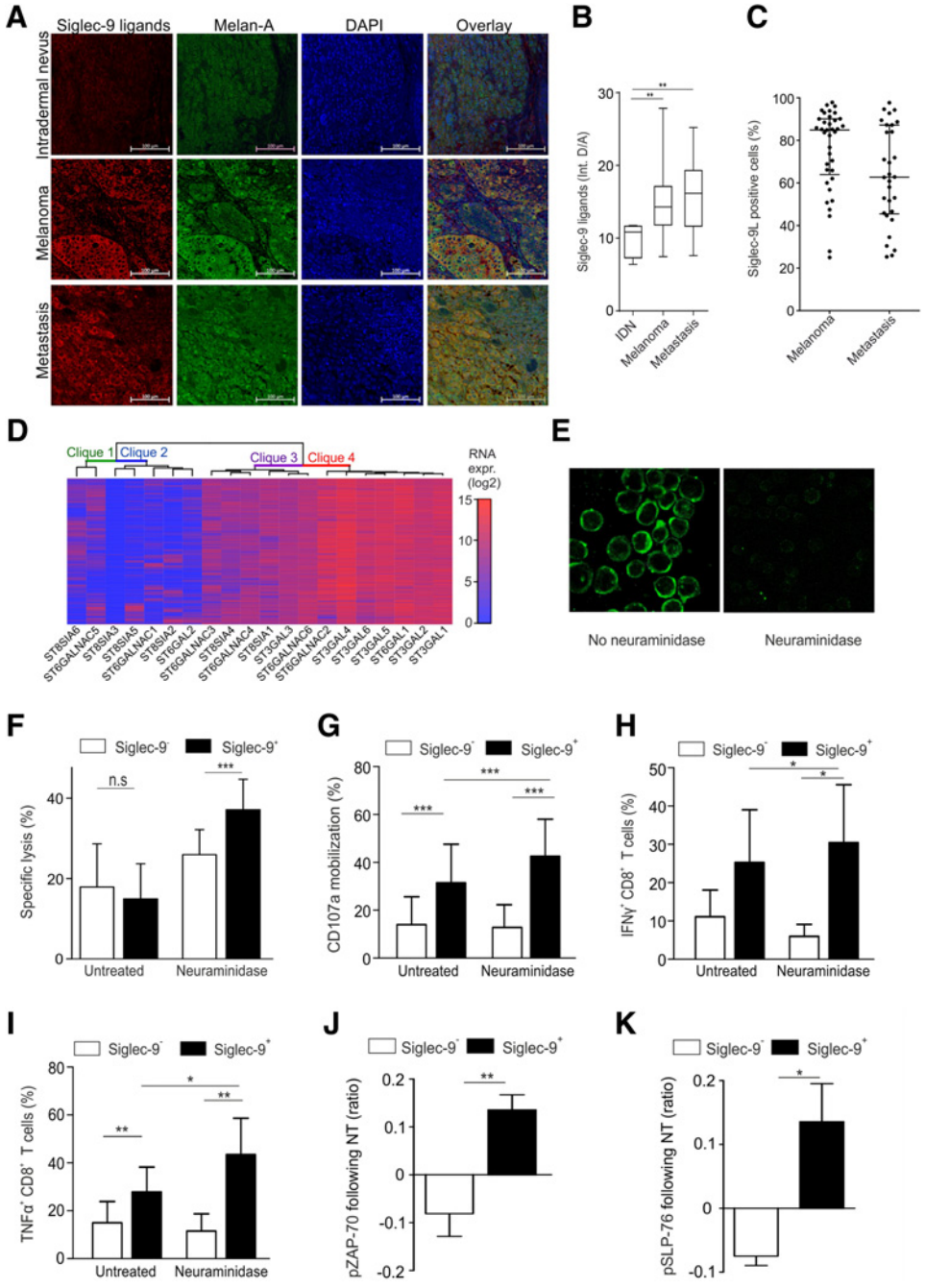

Figure 2.

Tumor expression of Siglec-9 ligands inhibits TCR signaling and effector functions of Siglec-9$^+$ CD8$^+$ T cells. **A** and **B,** IHC tissue microarray analysis (TMA) for Siglec-9 ligand expression in IDN; $n = 7$), primary melanoma ($n = 62$), and metastatic melanoma ($n = 20$). Representative examples costained with melanoma marker (**A**) melan-A and DAPI and (**B**) quantitative analysis (int. D/A: integrated density/tumor area) using box-and-whisker diagrams (median, lower, and upper quartiles; horizontal lines define minimum and maximum). **C,** IHC TMA analysis for Siglec-9 ligand$^+$ cancer cells in melanoma ($n = 37$) and metastatic melanoma ($n = 30$). Data, present median and interquartile range. **D,** RNA expression of sialyltransferases in melanoma ($n = 469$), based on TCGA Network data computed by a dendrogram clustering algorithm. Cliques' numbers are arbitrary given from left to right for an expression pattern rising from low to high RNA signal. **E,** Confocal immunofluorescence microscopy analysis indicating localization of Siglec-9 ligands on the surface of P815 cells with and without neuraminidase treatment (25 mU; sialic acid dependency). **F–K,** Target cell neuraminidase treatment effects on responses of redirected CD8$^+$ T-cell from healthy donors upon coculture with anti-CD3–loaded P815 tumor cells for (**F**) 4 or (**G–I**) 5 hours. **F,** Cytotoxicity, (**G**) CD107a mobilization, and (**H**) intracellular IFNγ or (**I**) TNFα production. **J** and **K,** Flow-cytometric monitoring of the phosphorylation status of intracellular TCR signaling molecules (**J**) pZAP-70 and (**K**) pSLP-76 upon exposure of T cells to anti-CD3–loaded P815 tumor cells for 10 minutes. Relative phosphorylation changes as a consequence of neuraminidase treatment (desialylation) are shown. **F–K,** Effector/target (E/T) ratio at 3:1. Statistical analysis was performed by one-way ANOVA followed by followed by (**B**) Holm–Sidak or (**F–H**) Bonferroni posttest or (**I–K**) Student *t* test. *, $P < 0.05$; **, $P < 0.01$; ***, $P < 0.001$; n.s., not significant. Error bars, SD. Data are representative of at least (**K**) 3, (**J**) 5, or (**F–H**) 6 experiments.

Published OnlineFirst April 15, 2019; DOI: 10.1158/2326-6066.CIR-18-0505

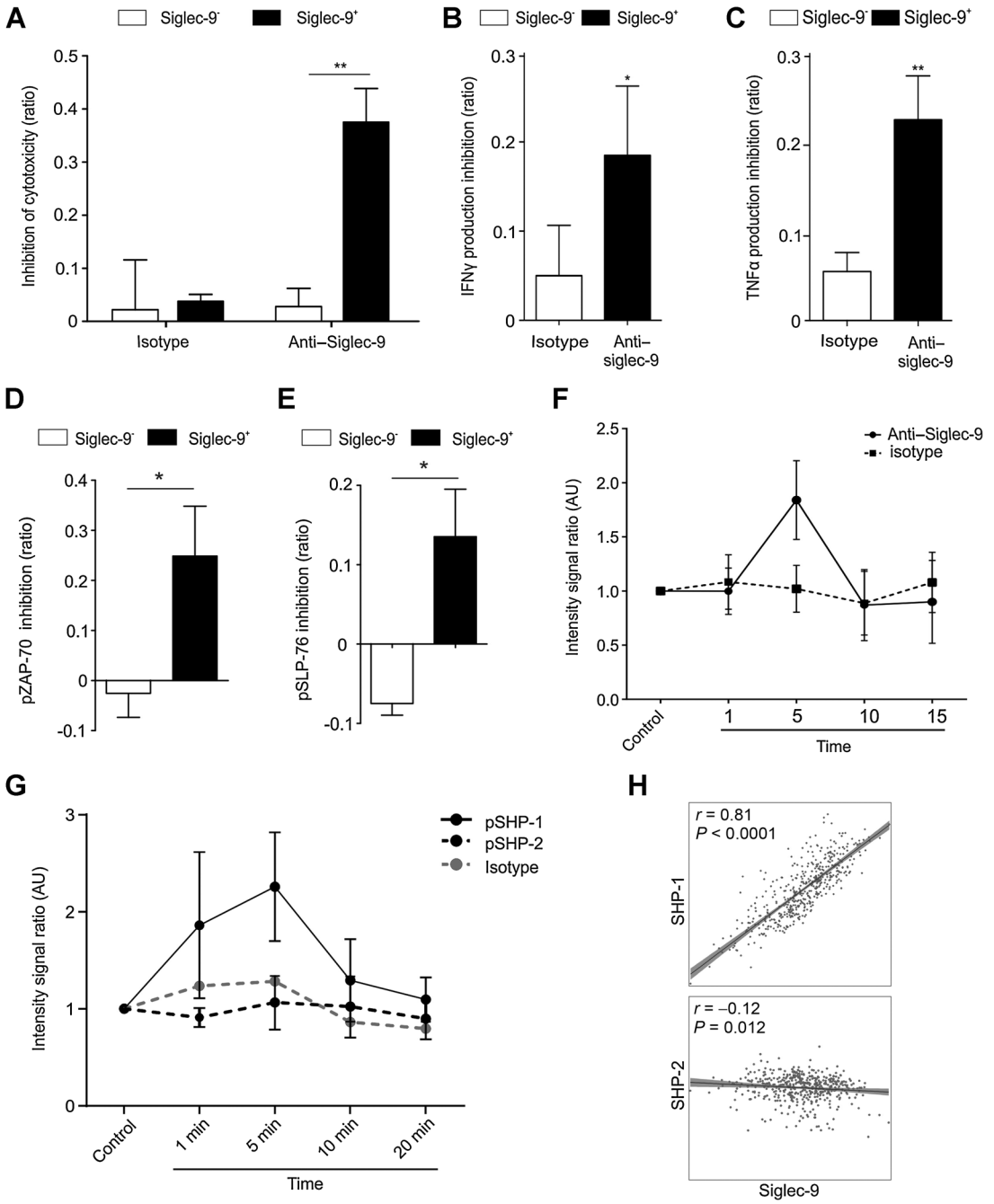

Figure 3.

Inhibition of TCR signaling and CD8$^+$ T-cell effector functions by Siglec-9$^+$ is associated with phosphorylation of SHP-1 but not SHP-2. **A,** Redirected cytotoxicity assay using healthy donor CD8$^+$ T cells against anti-CD3–loaded P815 tumor cells (3:1 E/T ratio) upon engagement by agonistic anti–Siglec-9 or mouse IgG1 as isotype control (3 μg/mL). **B** and **C,** Intracellular cytokine production of (**B**) IFNγ or (**C**) TNFα by healthy donor CD8$^+$ T cells upon engagement by agonistic anti–Siglec-9 (3 μg/mL) following 5 hours culture with anti-CD3 and anti-CD28 costimulation (both 1 μg/mL). **D** and **E,** Flow-cytometric monitoring of the phosphorylation status of intracellular TCR signaling molecules (**D**) pZAP-70 and (**E**) pSLP-76 upon healthy donor CD8$^+$ T-cell engagement by agonistic anti–Siglec-9 with costimulation by anti-CD3 and anti-CD28 (both 1 μg/mL). **F,** Phosphorylation status of Siglec-9 CD8$^+$ T cells from healthy donors treated with anti–Siglec-9 or isotype control (both 3 μg/mL) for 1 or 5, 10, and 15 minutes compared with time-matched controls (ratio) measured by ELISA. **G,** Densitometric analysis of immunoblots demonstrating SHP-1 or SHP-2 phosphorylation in CD8$^+$ T cells from healthy donors treated with anti–Siglec-9 or isotype control (both 3 μg/mL) for 1 or 5, 10, and 20 minutes compared with time-matched controls (ratio). **H,** Pairwise scatter plot representation of RNA expression (log2) of Siglec-9 compared with SHP-1 and SHP-2 in melanoma specimens ($n = 469$), according to TCGA Network data. Statistical analysis was performed by Student t test (**A–E**). *, $P < 0.05$; **, $P < 0.01$. Data are representative of at least (**D**) three or (**A–C, E, G**) four experiments.

Published OnlineFirst April 15, 2019; DOI: 10.1158/2326-6066.CIR-18-0505

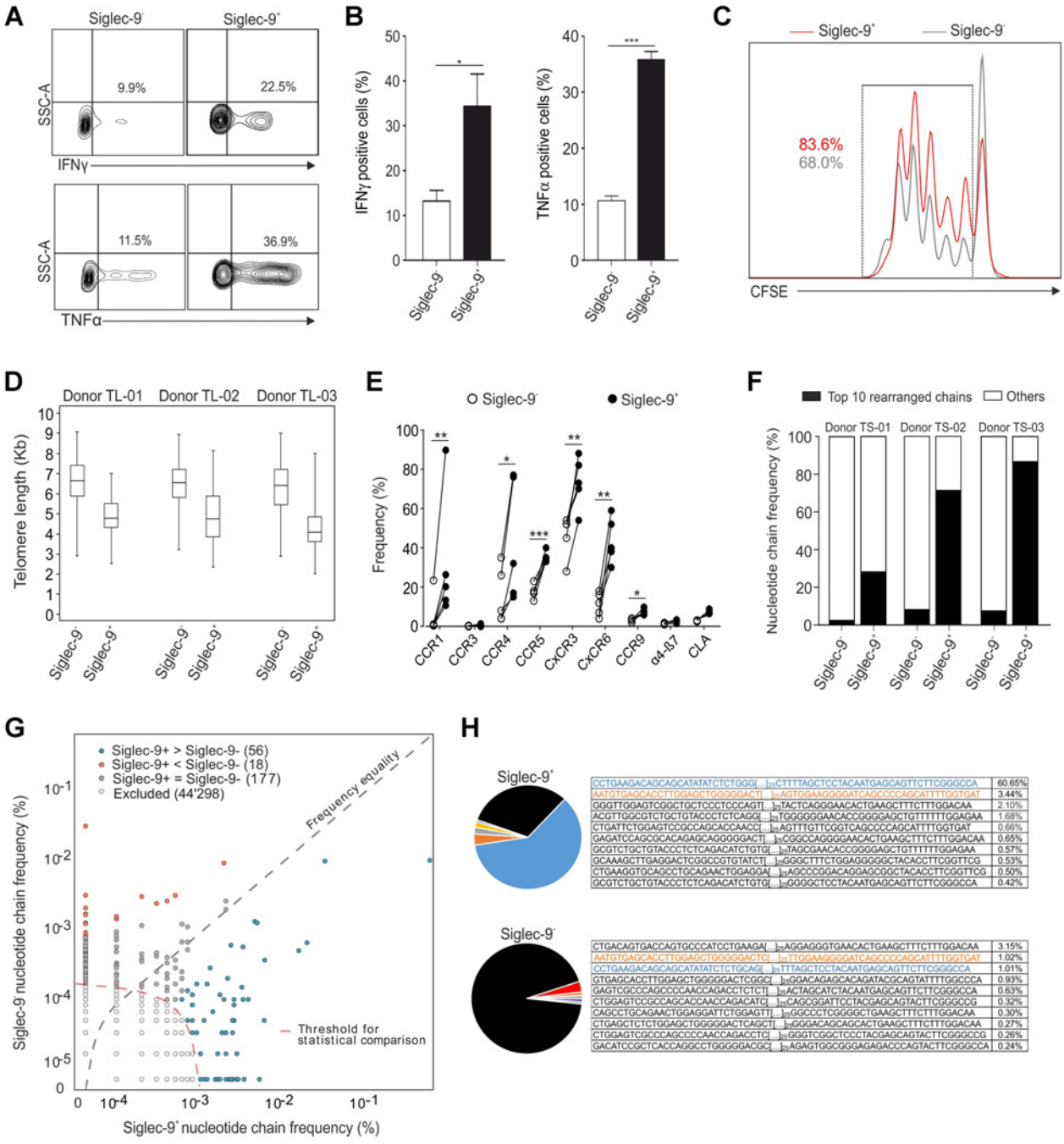

Figure 4.

Siglec-9$^+$ CD8$^+$ T-cell clonotypes, chemokine receptor expression, and function upon TCR stimulation *in vitro*. Analysis of peripheral blood CD8$^+$ T cell from healthy donors. **A,** Representative flow cytometry plots and (**B**) flow-cytometric quantitative analysis demonstrating intracellular IFNγ or TNFα production in CD8$^+$ T-cell subsets following 5 hours culture with costimulation by anti-CD3 and anti-CD28 (1 μg/mL). **C,** Representative flow-cytometric data illustrating proliferation of anti-CD3 and anti-CD28 (1 μg/mL) costimulated CD8$^+$ T-cell subsets, assessed 4 days after activation. **D,** Telomere length analysis of CD8$^+$ T-cell subsets from healthy donors. The box shows 25th to 75th percentiles with median; error bars, 1st to 99th percentiles. **E,** Flow-cytometric analysis of chemokine receptors on the surface of CD8$^+$ T-cell subsets. **F,** Frequency distribution of clonotypes based on the 10 most prevalent nucleotide TCRvβ chains within CD8$^+$ T-cell subsets of healthy donors. **G,** Nucleotide chain distribution of clonotype frequency in Siglec-9$^+$ CD8$^+$ T cells (*x*-axis) and Siglec-9$^-$ CD8$^+$ T cells (*y*-axis) from donor TS-02. Orange and blue dots represent clonotypes that were statistically found more frequently in one of these two populations based on Fisher exact test and are above the threshold for statistical comparison (red dotted line, indicating minimum cumulative number of templates). The black dotted line indicates frequency equality. **H,** Illustration of the 10 most expanded TCRvβ nucleotide chain distribution frequency in CD8$^+$ T-cell subsets isolated from donor TS-02. *, $P < 0.05$; **, $P < 0.01$; ***, $P < 0.001$, Student *t* test. Data are representative of at least (**E**) three, (**H**) five, or (**G**) six experiments.

Published OnlineFirst April 15, 2019; DOI: 10.1158/2326-6066.CIR-18-0505

in particular CCR5, CXCR3, and CXCR6, as determined by multiparametric flow cytometry (Fig. 4E).

To investigate the diversity of the TCR repertoire of Siglec-9$^+$ and Siglec-9$^-$ CD8$^+$ T-cell subsets from healthy peripheral blood, deep-sequencing of TCRVβ chains on genomic DNA was performed by multiplex PCR assays and then sequenced using the ImmunoSEQ immune profiling platform (35). The distribution of individual clonotypes was dissimilar between the CD8$^+$ T-cell subsets, with higher frequencies of the 10 top rearranged clones in the Siglec-9$^+$ CD8$^+$ T-cell subset (Fig. 4F). Despite the predominance of expanded clonotypes within the Siglec-9$^+$ CD8$^+$ T-cell subset, some nucleotide chain sequences were shared between Siglec-9$^+$ and Siglec-9$^-$ CD8$^+$ T cells, as illustrated in donor TS-02 (Fig. 4G and H), suggesting that Siglec-9 receptor expression can be acquired during the process of clonal expansion. However, polyclonal T-cell activation by CD3 and CD28 mAbs and combinations of different cytokines or tumor cell line supernatants did not induce significant Siglec-9 expression in sorted Siglec-9$^-$ cells from healthy donors (Supplementary Fig. S6). Together, these data provide evidence of a previous clonal expansion of Siglec-9$^+$ CD8$^+$ T cells and demonstrated the high proliferative and functional capacities of this CD8$^+$ T-cell subset.

Analysis of tumor-infiltrating Siglec-9$^+$ CD8$^+$ T cells

Using multiparametric flow cytometry, we examined the coexpression of Siglec-9 with known modulatory T-cell receptors, including immune checkpoints CTLA-4, PD-1, BTLA, LAG3, and Tim-3, on TILs from melanoma patients (Fig. 5A). Coexpression of Siglec-9 and PD-1 was frequent, which was also observed in healthy donor Siglec-9$^+$ CD8$^+$ T cells (Supplementary Fig. S7). A correlation between genes encoding Siglec-9, PD-1, and CD8α or CD8β was also observed in tumors based on the TCGA melanoma data set (Fig. 5B). The potential for functional redundancy between the Siglec-9 and PD-1 regulatory pathways was tested in the redirected cytotoxicity assay using CD8$^+$ T cells sorted from healthy donors against P815 cells, as these cells upregulate murine PD-L1 and, to a lesser extent, PD-L2 upon IFNγ stimulation (Supplementary Fig. S8), both of which are known ligands of human PD-1 (36, 37). In this setting, consistent with the observed coexpression pattern, Siglec-9$^+$ CD8$^+$ T cells, but not Siglec-9$^-$ cells, responded to treatment with the PD-1 checkpoint inhibitor pembrolizumab. The combined blockade resulted in synergistic effects on cytotoxicity (Fig. 5C). Deep-sequencing of the TCRVβ chains from these melanoma TILs revealed predominant clonotypes with co-occurrence in both Siglec-9$^+$ and Siglec-9$^-$ CD8$^+$ T-cell

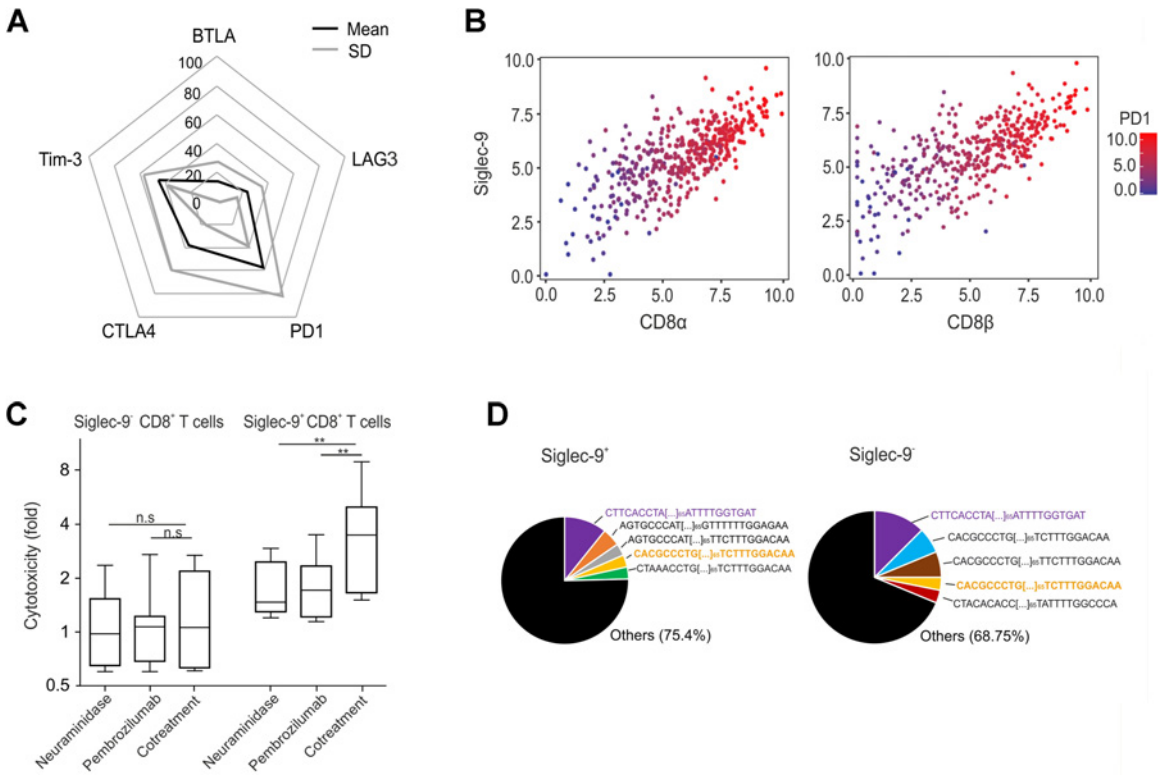

Figure 5.

Coinhibitory receptor expression and clonotype analysis of tumor-infiltrating Siglec-9$^+$ CD8$^+$ T cells in melanoma. **A,** Radar chart of flow-cytometric data demonstrating surface coexpression of Siglec-9 with PD-1, CTLA-4, BTLA, LAG3, or Tim-3 on CD8$^+$ T cells from melanoma TILs; $n = 4$). Black line, mean; gray lines, SD. **B,** Scatter diagram representation of RNA expression (log2) of Siglec-9, PD-1, and CD8α or CD8β in melanoma specimens ($n = 469$). Data are obtained from TCGA. **C,** Redirected cytotoxicity of healthy donor CD8$^+$ T cells against anti-CD3–loaded P815 tumor cells (3:1 E/T ratio) for 4 hours upon anti–PD-1 (10 μg/mL; pembrolizumab), target cell neuraminidase treatment (25 mU), or both. Plot represents median with 5–95 percentile whiskers. **D,** TCRvβ nucleotide chain distribution frequency in CD8$^+$ T-cell subsets isolated from the TILs of melanoma patient ($n = 1$). Statistical analysis was performed by one-way ANOVA followed by (**C**) Bonferroni posttest. **, $P < 0.01$; n.s., not significant. Data are representative of at least (**A**) four or (**C**) 9 experiments.

Published OnlineFirst April 15, 2019; DOI: 10.1158/2326-6066.CIR-18-0505

subsets (Fig. 5D), suggesting that Siglec-9 expression might be induced in the melanoma tumor microenvironment.

Discussion

In humans, as opposed to other hominids, only a minority of circulating human T cells express Siglecs (21, 22), which are glycan-binding receptors (lectins) that recognize sialic acid–containing glycans (sialoglycans).The role and relevance of Siglecs in the control of T cells and the characteristics of Siglec-expressing T cells remain unexplored. We observed that the majority of tumor-infiltrating CD8$^+$ T cells in all investigated melanoma tissues expressed Siglec-9. Siglec-expressing T cells in the tumors, but also their counterparts circulating at lower numbers in the peripheral blood of both melanoma patients and healthy individuals, predominantly consisted of EM cells. Further analysis confirmed the previous clonal expansion of Siglec-9$^+$ CD8$^+$ T cells, which exhibited T-cell effector functionality (38, 39). When stimulated using anti-CD3 and anti-CD28, Siglec-9$^+$ CD8$^+$ T cells had higher proliferation and responses compared with Siglec-9$^-$ CD8$^+$ T cells. On the other hand, engagement of the ITIM-containing Siglec-9 by anti–Siglec-9 significantly suppressed TCR signaling and effector functions, which was associated with phosphorylation of Siglec-9 and SHP-1, but not SHP-2, in human primary CD8$^+$ T cells. These results suggest that inhibitory Siglec-9–mediated signaling pathways may prevail over antibody-mediated sequestering effects. In line with this observation, in Jurkat cells, Siglec-9 has been shown to associate preferentially with SHP-1, and not SHP-2 (21). The preference for SHP-1 might contribute to the synergistic effects of concomitant PD-1 engagement, a receptor that also contains an ITIM and preferentially recruits SHP-2 in T cells (36, 40). In patients positively responding to pembrolizumab treatment, the blockade of Siglec-9 could enhance the host immune response against cancer and could represent an alternative target for patients with poor responses to pembrolizumab treatment. We observed coexpression of Siglec-9 with several known inhibitory T-cell receptors, e.g., PD-1, CTLA-4, and Tim-3, in healthy individuals and melanoma patients, with the highest correlation being with PD-1. Despite this inhibitory phenotype, functional responses of Siglec-9$^+$ CD8$^+$ T cells to CD3/CD28 costimulation were higher than those observed for their Siglec-9$^-$ counterparts *in vitro*. Based on the high expression of Siglec-9 ligands on most tumor cells in primary and metastatic melanoma specimens and the co-occurrence of Siglec-9 expression on the majority of intratumoral CD8$^+$ EM T cells, we propose a mechanism of tumor glycosylation-dependent immune resistance.

Approved immunotherapy agents include antibodies targeting key regulatory receptors on T cells, such as CTLA-4 and PD-1, that function to block the inhibitory receptor signaling that prevents effective antitumor responses (5). However, the clinical success of therapies targeting such immune checkpoints is limited to a subset of patients, and combination therapies to improve tumor responses (41, 42) often come at the cost of increased occurrence of immune-related adverse events (irAEs; refs. 43, 44). Clinical trials directed at empirically testing novel combinations have led to operational difficulties, such as competition in recruiting subjects, and the need for mechanism-based approaches to immune combinations has been recognized (1, 45). Conceptually, targeting immunologic checkpoints that include dominant regulatory circuits confined to the tumor microenvironment, such as Siglec-9 receptor–ligand interactions, might allow to selectively unleash the restricted repertoire of tumor-infiltrating T cells, while reducing the potential for uncontrolled T-cell activation and associated irAEs (43, 44).

The reported findings support evidence for an immunosuppressive role of tumor glycosylation (21, 22) by showing that tumor-intrinsic hypersialylation inhibits effector functions of Siglec-9$^+$ cytotoxic T cells, which represented the major fraction of intratumoral CD8$^+$ T cells in melanoma. The functional state of these cells combined with signatures of clonal expansion supports the concept that coinhibitory receptor expression on cytotoxic T cells may not be sufficient to distinguish exhaustion from activation (28). These results also suggest that Siglec-9$^+$ CD8$^+$ T cells may play a key role in adaptive immunity acquired during clonal expansion (28) and may reflect an inherent mechanism of resistance to immunotherapy. Diffuse expression of Siglec-9 ligands has also been observed in breast, lung, colon, and renal cancers, as well as leukemia (16, 17), suggesting that the Siglec-9 pathway may function as a checkpoint molecule in other cancers in addition to melanoma. Targeting the tumor-restricted establishment of the functional Siglec-9 receptor–ligand axis, resulting from the co-occurrence of specific tumor glycosylation patterns and clonally restricted, tumor-confined Siglec-9$^+$ cytotoxic T cells, may provide a strategy to improve immunotherapeutic treatments for cancer.

Data and materials availability: All data are available in the manuscript or the supplementary materials.

Disclosure of Potential Conflicts of Interest

A. Zippelius is a consultant/advisory board member for Bristol Myers Squibb, NBE Therapeutics, Secarna, Crescendo, MSD, Roche, and Hookipa and has received noncommercial research agreements with NBE Therapeutics, Secarna, ACM Pharma, Hookipa, Crescendo and Beyondsprings. H. Läubli reports receiving commercial research funding from and is a consultant/advisory board member for Palleon Pharmaceuticals. P. Romero is editor-in-chief of *Journal for Immunotherapy of Cancer*; reports receiving a commercial research grant from Roche pRED-Zurich; has received honoraria from the speakers bureau of Bristol-Myers Squibb, AstraZeneca, and Roche; and is a consultant/advisory board member for Immatics biotechnologies, NexImmune, and Transgene. No potential conflicts of interest were disclosed by the other authors.

Authors' Contributions

Conception and design: Q. Haas, C. Jandus, R.E. Hunger, H.-U. Simon, S. von Gunten

Development of methodology: Q. Haas, G.M. Baerlocher

Acquisition of data (provided animals, acquired and managed patients, provided facilities, etc.): Q. Haas, K.F. Boligan, C. Jandus, C. Schneider, S.M.S. Jafari, G.M. Baerlocher, H. Läubli, R.E. Hunger, P. Romero, H.-U. Simon

Analysis and interpretation of data (e.g., statistical analysis, biostatistics, computational analysis): K.F. Boligan, C. Jandus, C. Schneider, C. Simillion, A. Zippelius, G.M. Baerlocher, S. von Gunten

Writing, review, and/or revision of the manuscript: Q. Haas, K.F. Boligan, C. Jandus, C. Schneider, M.A. Stanczak, S.M.S. Jafari, A. Zippelius, G.M. Baerlocher, R.E. Hunger, P. Romero, H.-U. Simon, S. von Gunten

Administrative, technical, or material support (i.e., reporting or organizing data, constructing databases): Q. Haas, M.A. Stanczak, S.M.S. Jafari, A. Zippelius, G.M. Baerlocher, H. Läubli, R.E. Hunger, H.-U. Simon, S. von Gunten

Study supervision: Q. Haas, S. von Gunten

Acknowledgments

We thank Ingrid Helsen for technical assistance. Research in the laboratory of S.V.G was supported by Swiss National Science Foundation (SNSF) grants 310030_162552 and 310030_184757, by the Swiss Cancer League/Swiss Cancer Research grants KFS-3941-08-2016 and KFS-3248-08-2013, the Novartis Foundation for medical-biological research, and Palleon Pharmaceuticals Inc., Waltham MA (USA). H.-U. Simon received support from the Swiss National

Science Foundation (grants No. 310030-166473 and 310030_184816) and the European Union's Horizon 2020 research and innovation program (Marie Sklodowska-Curie grant No. 642295; MEL-PLEX). C. Jandus received support by the SNSF (PMPDP3_129022, Marie-Heim Vögtlin Program and PZ00P3_161459, Ambizione Program).

The costs of publication of this article were defrayed in part by the payment of page charges. This article must therefore be hereby marked *advertisement* in accordance with 18 U.S.C. Section 1734 solely to indicate this fact.

Received July 25, 2018; revised December 10, 2018; accepted April 8, 2019; published first April 15, 2019.

References

1. Ribas A, Wolchok JD. Cancer immunotherapy using checkpoint blockade. Science 2018;359:1350–5.
2. Couzin-Frankel J. Breakthrough of the year 2013. Cancer Immunotherapy Science 2013;342:1432–3.
3. Chen DS, Mellman I. Elements of cancer immunity and the cancer–immune set point. Nature 2017;541:321–30.
4. Sharma P, Hu-Lieskovan S, Wargo JA, Ribas A. Primary, adaptive, and acquired resistance to cancer immunotherapy. Cell 2017;168:707–23.
5. Sharma P, Allison JP. The future of immune checkpoint therapy. Science 2015;348:56–61.
6. Sharma P, Allison JP. Immune checkpoint targeting in cancer therapy: Toward combination strategies with curative potential. Cell 2015;161: 205–14.
7. Jerby-Arnon L, Shah P, Cuoco MS, Rodman C, Su M-J, Melms JC, et al. A cancer cell program promotes T cell exclusion and resistance to checkpoint blockade. Cell 2018;175:984–997.
8. O'Donnell JS, Long GV, Scolyer RA, Teng MW, Smyth MJ. Resistance to PD1/PDL1 checkpoint inhibition. Cancer Treat Rev 2017;52:71–81.
9. Stowell SR, Ju T, Cummings RD. Protein glycosylation in cancer. Annu Rev Pathol Mech Dis 2015;10:473–510.
10. Boligan KF, Mesa C, Fernandez LE, Von Gunten S. Cancer intelligence acquired (CIA): tumor glycosylation and sialylation codes dismantling antitumor defense. Cell Mol Life Sci 2015;72:1231–48.
11. Fuster MM, Esko JD. The sweet and sour of cancer: glycans as novel therapeutic targets. Nat Rev Cancer 2005;5:526–42.
12. Varki A. Since there are PAMPs and DAMPs, there must be SAMPs? Glycan "self-associated molecular patterns" dampen innate immunity, but pathogens can mimic them. Glycobiology 2011;21:1121–4.
13. Crocker PR, Paulson JC, Varki A. Siglecs and their roles in the immune system. Nat Rev Immunol. 2007;7:255–66.
14. Jandus C, Simon H-U, von Gunten S. Targeting Siglecs—A novel pharmacological strategy for immuno- and glycotherapy. Biochem Pharmacol 2011;82:323–32.
15. Hudak JE, Canham SM, Bertozzi CR. Glycocalyx engineering reveals a Siglec-based mechanism for NK cell immunoevasion. Nat Chem Biol 2014; 10:69–75.
16. Jandus C, Boligan KF, Chijioke O, Liu H, Dahlhaus M, Démoulins T, et al. Interactions between Siglec-7/9 receptors and ligands influence NK cell – dependent tumor immunosurveillance. J Clin Invest 2014;124:1810–20.
17. Läubli H, Pearce OMT, Schwarz F, Siddiqui SS, Deng L, Stanczak MA, et al. Engagement of myelomonocytic Siglecs by tumor-associated ligands modulates the innate immune response to cancer. Proc Natl Acad Sci 2014;111: 14211–6. 9
18. Beatson R, Tajadura-Ortega V, Achkova D, Picco G, Tsourouktsoglou T-D, Klausing S, et al. The mucin MUC1 modulates the tumor immunological microenvironment through engagement of the lectin Siglec-9. Nat Immunol 2016;17:1273–81.
19. Adams OJ, Stanczak MA, von Gunten S, Läubli H. Targeting sialic acid–Siglec interactions to reverse immune suppression in cancer. Glycobiology 2017;28:640–47
20. Haas Q, Simillion C, von Gunten S. A cartography of siglecs and sialyltransferases in gynecologic malignancies: is there a road towards a sweet future? Front Oncol 2018;8:68.
21. Ikehara Y, Ikehara SK, Paulson JC. Negative regulation of T cell receptor signaling by Siglec-7 (p70/AIRM) and Siglec-9. J Biol Chem 2004;279: 43117–25.
22. Nguyen DH, Tangvoranuntakul P, Varki A. Effects of natural human antibodies against a nonhuman sialic acid that metabolically incorporates into activated and malignant immune cells. J Immunol 2005;175:228–36.
23. Varki A. Glycan-based interactions involving vertebrate sialic-acid-recognizing proteins. Nature 2007;446:1023–9.
24. Bankhead P, Loughrey MB, Fernández JA, Dombrowski Y, McArt DG, Dunne PD, et al. QuPath: open source software for digital pathology image analysis. Sci Rep 2017;7:16878.
25. Appay V, Douek DC, Price DA. CD8+T cell efficacy in vaccination and disease. Nat Med 2008;14:623–8.
26. Palucka AK, Coussens LM. The basis of oncoimmunology. Cell 2016;164: 1233–47.
27. Geginat J, Lanzavecchia A, Sallusto F. Proliferation and differentiation potential of human CD8+ memory T-cell subsets in response to antigen or homeostatic cytokines. Blood 2003;101:4260–6.
28. Tirosh I, Izar B, Prakadan SM, Wadsworth MH, Treacy D, Trombetta JJ, et al. Dissecting the multicellular ecosystem of metastatic melanoma by single-cell RNA-seq. Science 2016;352:189–96.
29. Wherry EJ, Ha S-J, Kaech SM, Haining WN, Sarkar S, Kalia V, et al. Molecular signature of CD8+ T cell exhaustion during chronic viral infection. Immunity 2007;27:670–84.
30. Fuertes Marraco SA, Neubert NJ, Verdeil G, Speiser DE. Inhibitory receptors beyond T cell exhaustion. Front Immunol 2015;6:310.
31. Crocker PR, Paulson JC, Varki A. Siglecs and their roles in the immune system. Nat Rev Immunol 2007;7:255–66.
32. von Gunten S, Yousefi S, Seitz M, Jakob SM, Schaffner T, Seger R, et al. Siglec-9 transduces apoptotic and nonapoptotic death signals into neutrophils depending on the proinflammatory cytokine environment. Blood 2005;106:1423–31.
33. Macauley MS, Crocker PR, Paulson JC. Siglec-mediated regulation of immune cell function in disease. Nat Rev Immunol 2014;14:653–66.
34. Baerlocher GM, Vulto I, de Jong G, Lansdorp PM. Flow cytometry and FISH to measure the average length of telomeres (flow FISH). Nat Protoc 2006;1: 2365–76.
35. Becattini S, Latorre D, Mele F, Foglierini M, De Gregorio C, Cassotta A, et al. Functional heterogeneity of human memory CD4+T cell clones primed by pathogens or vaccines. Science 2015;347:400–6.
36. Latchman Y, Wood CR, Chernova T, Chaudhary D, Borde M, Chernova I, et al. PD-L2 is a second ligand for PD-1 and inhibits T cell activation. Nat Immunol 2001;2:261–8.
37. Freeman GJ, Long AJ, Iwai Y, Bourque K, Chernova T, Nishimura H, et al. Engagement of the PD-1 immunoinhibitory receptor by a novel B7 family member leads to negative regulation of lymphocyte activation. J Exp Med 2000;192:1027–34.
38. Haas A, Weckbecker G, Welzenbach K. Intracellular phospho-flow cytometry reveals novel insights into TCR proximal signaling events. A comparison with Western blot. Cytom Part A 2008;73:799–807.
39. Hogan SA, Courtier A, Cheng PF, Jaberg-Bentele NF, Goldinger SM, Manuel M, et al. Peripheral blood TCR repertoire profiling may facilitate patient stratification for immunotherapy against melanoma. Cancer Immunol Res 2018;4:959–67.
40. Chemnitz JM, Parry RV, Nichols KE, June CH, Riley JL. SHP-1 and SHP-2 associate with immunoreceptor tyrosine-based switch motif of programmed death 1 upon primary human T cell stimulation, but only receptor ligation prevents T cell activation. J Immunol 2004;173:945–54.
41. Sharma P, Allison JP. Immune checkpoint targeting in cancer therapy: toward combination strategies with curative potential. Cell 2015;161: 205–14.
42. Schmidt C. The benefits of immunotherapy combinations. Nature 2017; 552:S67–9.
43. Boutros C, Tarhini A, Routier E, Lambotte O, Ladurie FL, Carbonnel F, et al. Safety profiles of anti-CTLA-4 and anti-PD-1 antibodies alone and in combination. Nat Rev Clin Oncol 2016;13:473–86.
44. Sanmamed MF, Chen L. A paradigm shift in cancer immunotherapy: from enhancement to normalization. Cell 2018;175:313–26.
45. Kaiser J. Too much of a good thing? Science 2018;359:1346–7.

AACR American Association for Cancer Research

Cancer Immunology Research

Siglec-9 Regulates an Effector Memory CD8$^+$ T-cell Subset That Congregates in the Melanoma Tumor Microenvironment

Quentin Haas, Kayluz Frias Boligan, Camilla Jandus, et al.

Cancer Immunol Res Published OnlineFirst April 15, 2019.